Computer-Aided Civil and Infrastructure Engineering **26** (2011) 560–579

INDUSTRIAL APPLICATION

Wireless Monitoring of a Multispan Bridge Superstructure for Diagnostic Load Testing and System Identification

Michael V. Gangone

Graduate Research Assistant, Civil and Environmental Engineering, Clarkson University, 8 Clarkson Avenue Box 5712, Potsdam, NY 13699, USA

Matthew J. Whelan

Assistant Professor, Department of Civil and Environmental Engineering, University of North Carolina at Charlotte, 9201 University City Boulevard, Charlotte, NC 28223, USA

&

Kerop D. Janoyan*

Associate Professor, Civil and Environmental Engineering, Clarkson University, 8 Clarkson Avenue Box 5710, Potsdam, NY 13699, USA

Abstract: *This article focuses on the deployment of a wireless sensor system (WSS) developed at Clarkson University for structural monitoring purposes. The WSS is designed specifically for diagnostic bridge monitoring, providing independent conditioning for accelerometers, strain transducers, and temperature sensors in addition to high-rate wireless data transmission and is capable of supporting large-scale sensor arrays. A three-span simply supported structure was subjected to diagnostic load testing as well as ambient vibration monitoring. A total of 90 wireless and several wired sensors, including accelerometers and strain transducers were used in the deployment. Strain measurements provided capacity and demand characteristics of the structure in the form of neutral axis locations, load distributions, and dynamic allowances which ultimately produced an inventory and operating load rating for the structure. Additionally, modal characteristics of the structure, including natural frequencies and mode shapes, were derived from measured accelerations and discussed briefly.*

*To whom correspondence should be addressed. Email: *kerop@clarkson.edu*.

DOI: 10.1111/j.1467-8667.2010.00711.x

1 INTRODUCTION

As a significant portion of the aging network of highway bridges have met or exceeded their intended design lifetime and service limits, highway administrations are faced with the challenging task of allocating limited resources for replacement and rehabilitation of structures most critical for repair while managing the remaining end-of-life bridges without jeopardizing public safety. As demonstrated in the aftermath of recent bridge collapses over the past several decades, current schedule-based visual inspections can occasionally fall short of ensuring a safe operational model for highway bridge management with bridge closures preceding imminent failure. The increase in demand on highway infrastructure has coincided with the aging of a substantial percentage of the in-service national bridge inventory

creating greater urgency for quantitatively determining both the capacity and service limits of highway infrastructure. As with all mechanical systems, bridge components deteriorate over time due to the effects of weathering and stress cycling. This deterioration results in a reduction in the design performance that can ultimately progress to structural failure. As of 2009, an estimated 24% of the nation's over 600,000 bridges are currently classified as structurally deficient or functionally obsolete (12% structural deficient) by the federal highway administration (FHWA) (FHWA, 2009). This suggests that accuracy and reliability of bridge inspections is imperative and advanced quantitative methods to locate and repair the damage are of pressing importance.

Local, visual evaluations are often inadequate in that they may not always accurately reflect the true performance state of bridge components or the global condition of the entire bridge. Subjectivity on the part of the inspection team is a critical and unaddressed obstacle to the effectiveness of the bridge inspection program. Additionally, time and access to the structure are generally cited as issues routinely encountered during the evaluation of bridges. Structural components are not always easily accessible to the inspector and, therefore, cannot be assessed nor contribute toward the overall rating of the structure. Many times these elements, whether primary or secondary, are critical to the overall performance, load capacity, and structural response. With time being of the essence, the level of detail and proper attention given to each and every element is often overlooked and inspectors are prone to assuming the condition of most members is average. In 2001, the FHWA conducted a study which found that 56% of medium- to short-span bridges given an average condition rating were improperly assessed (Phares et al., 2001). The introduction of quantitative, measurement-based evaluation methods into the existing inspection framework will undoubtedly overcome the subjectivity and physical constraints limiting the effectiveness of the bridge inspection program.

Acceleration and strain measuring devices are two of the more common sensor types deployed for typical bridge monitoring. Currently, many state transportation agencies including the New York State Department of Transportation (NYSDOT) utilize diagnostic load testing with strain transducers to measure the performance and capacity of a bridge (Hag-Elsafi and Kunin, 2006). Load distribution, dynamic impact factors, end-fixity levels, and composite action between the deck and girders are evaluated to quantify the structural stiffness as well as load transfer and redundancy of the system and can either verify a design method or indicate the level of service life remaining in the structure. Accelerometers capture the dynamic response of the structure under ambient and forced vibrations allowing for, among other things, the determination of the modal properties (mode shapes, damping ratios and natural frequencies). Whether utilizing global or local monitoring methodologies, providing a greater number of sensors and sensor types (i.e., accelerometers, strain transducers, thermocouples, etc.) generally results in an improved overall representation of the structural performance.

Researchers are working to develop methods of structural monitoring to allow the complete and accurate assessment of structural performance in a nondestructive manner. DeWolf et al. (2006) monitored a series of bridges within the state of Connecticut, including a steel truss bridge, using wireless strain gages, and accelerometers. Wireless sensors were chosen due to the long span lengths and difficulty of instrumenting a cabled system over the long span lengths. Lynch et al. (2006) deployed a wireless system on the Geumdang Bridge in South Korea. Test vehicles provided an input loading to the concrete box girder bridge although acceleration measurements reveal the modal characteristics of the structure. Whelan et al. (2010) deployed 60 channels of wireless acceleration measurements over two networks of a 360 ft three-span continuous bridge superstructure. The measurements were sampled in real time and served to estimate the various modal characteristics of the structure including natural frequencies and mode shapes. Gangone et al. (2009) deployed 11 channels of strain data on an integral abutment bridge obtaining various load testing parameters. Bridge Diagnostics Incorporated (BDI) (2008) has recently developed a wireless strain-based system for bridge monitoring.

Although various research and commercial systems have been developed and implemented, methodologies of detecting and locating damage are of the utmost importance to any health monitoring system. To date many structural health monitoring (SHM) techniques rely on data gathered from vibrational measurements. An extensive review of these methods can be found in Sohn et al. (2003), Doebling et al. (1996), Humar et al. (2006), and Hsieh et al. (2006). Jang et al. (2008) utilized a damage locating vector (DLV) to detect damage on a laboratory truss structure. Shenton and Chajes (1999) deployed a SHM system on the first polymer composite bridge in Delaware, measuring the strain, deflections, temperature, and humidity of the structure. Cruz and Salgado (2009) evaluated six vibration-based damage detection methods using data collected from two different bridges undergoing different conditions of cracking and under various measurement noise levels. He et al. (2008) completed modal identification of the Vincent Thomas Bridge located in San Pedro, California based on a wind excitation

model and a calibrated finite element (FE) model. Realistic damage scenarios were implemented into the model for determining their effect on the structure's performance. Parks et al. (2007) discussed using terrestrial laser scanning (TLS) to measure the deformations of an entire structure for health monitoring purposes. Jiang et al. (2007) developed a "*Bayesian discrete wavelet packet transform denoising approach*" to reduce the noise in measured data for improved structural identification. Adeli and Jiang (2006) developed a dynamic time-delay fuzzy wavelet neural network (WNN) model for nonparametric identification of structures using the *nonlinear autoregressive moving average with exogenous inputs approach*. An adaptive Levenberg–Marquardt-least squares algorithm with a backtracking inexact linear search scheme was developed for training of the dynamic fuzzy WNN model (Jiang and Adeli, 2005). Jiang and Adeli (2005) present a model for damage detection of high-rise building structures subjected to seismic excitations using the dynamic fuzzy WNN model developed by the authors. They also propose a new damage evaluation method based on a power density spectrum method, called *pseudospectrum*. Jiang and Adeli (2008a) also present a dynamic fuzzy wavelet neuroemulator for nonlinear control of irregular high-rise building structures. They developed a neuro-genetic algorithm for finding the optimal control forces (Jiang and Adeli, 2008b).

Load testing and performance monitoring systems have been employed by numerous researchers as well. Significant research on health monitoring of structures has been published in this journal in recent years (Moaveni et al., 2009; Umesha et al., 2009; Huang et al., 2009; Chen and Liu, 2010; Huang et al., 2010). Chakraborty and DeWolf (2006) developed a strain monitoring system for evaluating a multispan bridge superstructure in the state of Connecticut. Chajes et al. (1997) performed an experimental load rating on a three-span bridge to determine if the current load posting of the bridge was necessary. Howell and Shenton III (2006) developed a near real-time web-based monitoring system for monitoring the strain response in a bridge. Jáuregui and Barr (2004) performed a diagnostic load test on a bridge in Albuquerque, New Mexico to determine the validity of the bridge rating and if additional overweight permits for trucks crossing the bridge could be issued. Soyoz and Feng (2009) deployed 13 accelerometers on the superstructure and columns of the Jamboree Road Over-Crossing, a three-span prestressed post-tensioned concrete box girder bridge. Wireless measurements were acquired over a 5-year period for determining a change in the mass and stiffness of the bridge in addition to soil spring values based on neural network techniques. Xu et al. (2007) used "direct soft parametric identification (DSPI)" and free vibrating strain measurements on a truss bridge to measure member stiffness and damping parameters.

Fig. 1. Wireless sensor system (WSS) node with accelerometer and strain transducer.

This article focuses on the deployment of a Wireless Sensor System (WSS) on a three-span simply supported bridge in Waddington, NY. Modal and strain-based characteristics of the superstructure were acquired through measurements taken from 99 different sensors over a 2-day period. The results provide a quantitative assessment into the structural performance of the bridge. Discussed primarily is the load testing and rating of the superstructure from strain measurements.

2 WIRELESS SENSOR NETWORK-BASED BRIDGE MONITORING

The WSS developed within the Laboratory for Intelligent Infrastructure and Transportation Technologies (LIITT) at Clarkson University was designed as a universal platform for high-rate, large-scale monitoring of the structural response (Figure 1). The sensor network is composed of an array of distributed sensing nodes that interface with sensors (i.e., accelerometers, strain transducers, temperature sensors), condition the analog signals, then convert them to digital readings, and transmit the data to a base coordinator. The base coordinator features the same wireless transceiver hardware as the remote nodes; however, its embedded functionality is to control high-rate, bi-directional wireless communications between the host computer and the distributed sensing units. The base coordinator is connected to the host computer across a universal serial bus (USB) connection using the communications device class to present the interface as a virtual COM port. This physical hardware interface is advantageous as it enables either network control from a CPU local to the measurement site or remote access across an internet connection through TCP/IP protocol using a

network-enabled USB hub. The primary hardware issues addressed in design of the wireless sensing units were appropriate signal conditioning for the range of responses typical for the spectrum of highway bridge designs and span-lengths, minimized power consumption for battery resource conservation, and high-throughput for large-scale network communications. A total of 30 wireless units, consisting of a dual-axis accelerometer, strain transducer and the custom conditioning and data acquisition system were developed and used in the monitoring. A more in-depth and exhaustive discussion of the developed wireless system can be found in Whelan and Janoyan (2009) and Whelan et al. (2009).

3 WIRELESS SENSOR FIELD DEPLOYMENT

3.1 Test structure

The highway bridge investigated, located on RT345 in upstate New York, consists of a 19.1 cm (7.5 in) thick reinforced concrete slab supported by three interior W33×152 and two W33×131 exterior steel girders over each span (Figure 2). By visual inspection of the bridge plans, it does not appear that composite action between the steel girders and reinforced concrete deck was a design consideration as shear stud connections are not present nor is the top flange embedded into the bridge deck. The bridge is a two-lane structure consisting of three 13.7 m (45 ft) simply supported spans carrying a total span of 41.7 m (137 ft) at an elevation of approximately 1.2 m (4 ft) from the waterline. The girders have a center-to-center spacing of 2.1 m (7 ft) and are supported by fixed and rocker steel bearings. End and midspan intermediate diaphragms are constructed of C15×33.9 sections that are bolted to transverse plates welded to the girders. Prior to the scheduled closure for replacement, the structure serviced New York State Route 345 over Big Sucker Brook in the town of Waddington. Constructed in 1957, the bridge maintained a sufficiency rating of 61.2%, an operational rating of 44.5 metric tons, and an average daily traffic estimate of 1,169 vehicles. The bridge is "R Posted" by New York State, indicating the "bridge does not have reserve capacity to accommodate most vehicles over legal weights, but can still safely carry legal weights" (NYSDOT, 2010). Testing described in this article was completed over a 2-day period where the first day consisted of output-only modal testing through acceleration measurements, and the following day a diagnostic load test using 2-H trucks (AASHTO, 2002) each weighing 21.75 metric tons (23.97 tons) for recording strain measurements.

3.2 Instrumentation

The bridge was instrumented at 30 locations over the three spans with dual-axis accelerometers for a total of 60 vibration measurement axes (Figure 3a). The use of a large number of stationary accelerometers enables simultaneous collection of vibration time histories across the structure. This is advantageous to using a roving system with reference accelerometers as it ensures consistent temperature, ambient vibration spectral characteristics, and consistent traffic loading. Furthermore, a stationary array would be necessary for permanent installation, so the deployment validates the ability of the network to deliver the required bandwidth for a long-term network infrastructure. Sampling durations of three minutes were collected in real-time of the digitally filtered analog to digital converter (ADC) conversions measured at 512 samples per second (Sps) and downsampled to a per channel rate of 128 Sps for transmission. An oversampling approach is implemented within the embedded software during the acquisition of measurements from the 12-bit ADC to increase the effective resolution of the conversion as well as to virtually eliminate signal attenuation in the measured bandwidth. Sensor data are oversampled and then passed through a digital low-pass filter prior to downsampling to the desired effective data rate that is transmitted across the radio. The digital filter is a 56th-order equiripple design implemented by the embedded software with the microcontroller hardware multiplier (Whelan and Janoyan, 2009). The use of oversampling reduces the effect of ADC quantization noise and is generally accepted to provide an additional bit of effective resolution for each power of four rate of oversampling.

On the subsequent day of testing, 30 strain transducers were installed across the structure for interfacing with the wireless sensor nodes with an additional 9 wired transducers monitoring bearing restraint of selected girders in the south and center spans and the bottom flange at midspan of girder 2 (G2) (Figure 3b). Nine wired sensors were required because there were only 30 available wireless nodes for testing and 39 locations of interest. The BDI transducers are Wheatstone full bridge resistive sensors housed in a durable, reusable transducer package that is mounted to the structure using bolted tabs and have a gauge length of 7.62 cm (3 in). The instrumentation layout devised is typical of experimental load ratings (Hag-Elsafi and Kunin, 2006). Placement of gauges at the top and bottom flange of a girder at the same longitudinal location facilitates determination of the neutral axis (NA) of bending. Gauges at the midspan of each girder enable distribution factors (DF) to be recorded for each load case, which

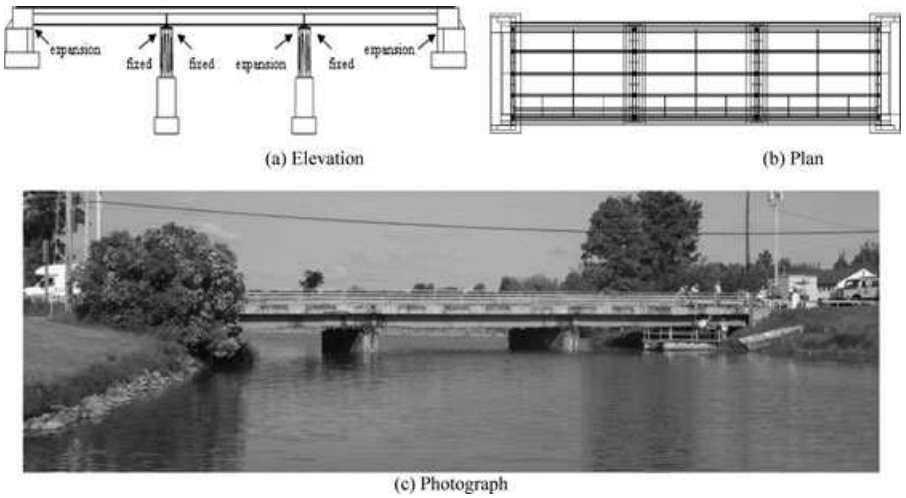

Fig. 2. Test structure: RT345 Bridge over Big Sucker Brook.

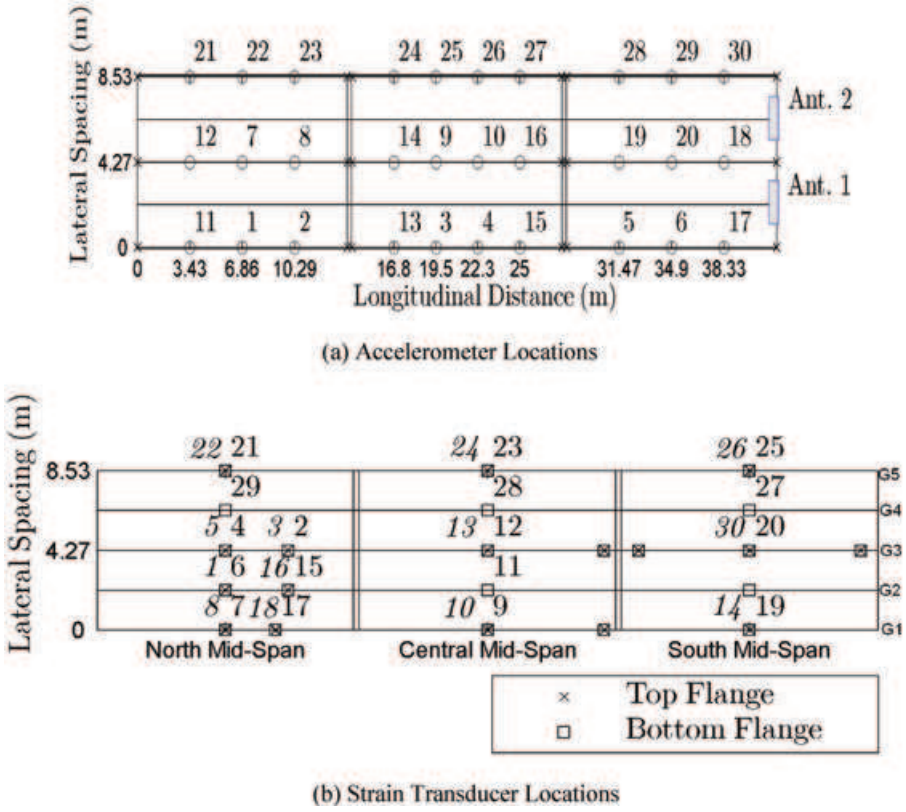

Fig. 3. Instrumentation layout for testing performed at the RT345 Bridge site.

indicate load shedding paths. Additionally, impact factors were computed from dynamic strain measurements. As in the case of vibration monitoring, the measurements were sampled at 128 Sps and transmitted in real-time to the network coordinator over test durations of three minutes. For these measurements, a signal gain of 420 V/V was applied to the analog signal and analog-to-digital conversion was performed using a first-order 15-bit charge-balancing ADC for sub-microstrain resolution of the sensor response.

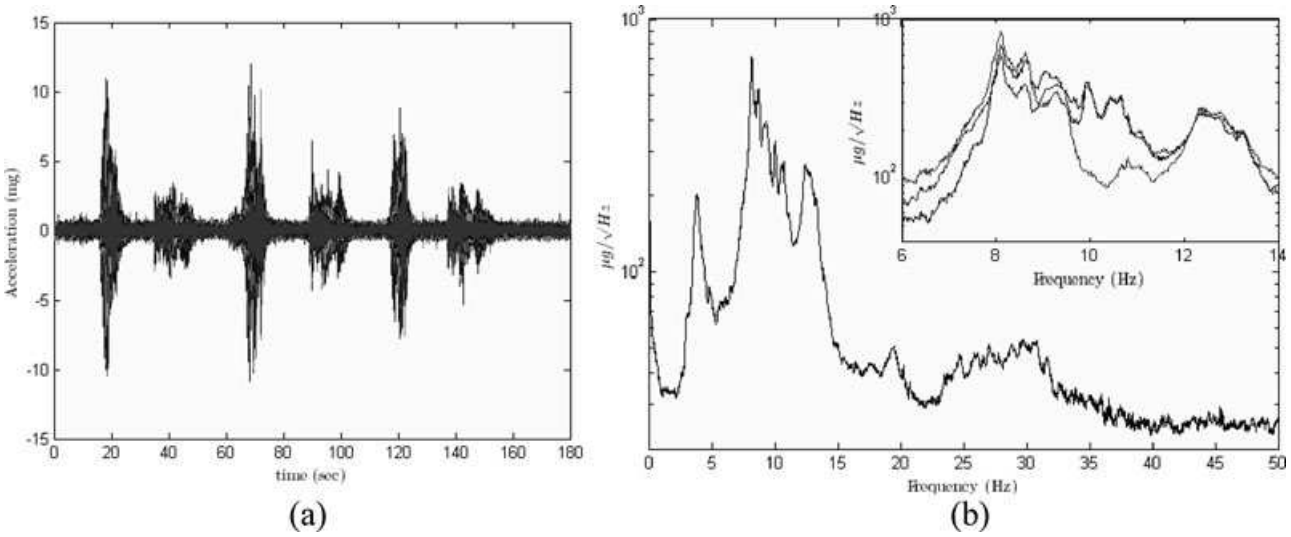

Fig. 4. (a) Typical vertical acceleration time history overlay from truck passes; (b) spectral content from distributed vibration measurements (overlay of individual average spectrums from each span within bandwidth of primary modes).

4 ANALYSIS OF RESULTS

4.1 Operational modal analysis

Two simultaneously operating wireless sensor networks in star topologies were deployed on the RT345 Bridge to enable the collection of vibration time histories from 60 accelerometers. As the bridge was closed to normal vehicular traffic, ambient traffic excitation was provided by means of a large truck that started from rest just ahead of one abutment, traveled across the bridge at approximately 16.1–24.1 km/h (10–15 mph), and then returned in reverse. During the operational modal analysis, the truck made passes in both lanes as well as down the centerline of the bridge. A typical acceleration time history reveals peak accelerations generally in the range of 10–15 mg (Figure 4a). The relatively sparse placement of sensors across the entire structure limits the effectiveness of the modal analysis to primarily the lower order bending modes, though there are a significant number of modes that can be reconstructed from such an instrumentation layout. The average normalized power spectral density revealed that the first-order natural frequencies of the spans resulting from vertical modes were generally in the range of 8 Hz–13 Hz (Figure 4b). This portion of the spectrum contains a dense cluster of four unique natural frequencies per each of the three spans. Additionally, it should be noted that there is a clear spike present at approximately 4 Hz in the average normalized power spectral density resulting from a lateral mode in each span. The energy provided from the slight vertical motion of this mode is captured in the spectrum; however, it is not a vertical mode. This was confirmed from subsequent FE analysis. Modal parameters were estimated from application of stochastic subspace identification and presented in Figure 5 for the vertical modes. The mode shapes and spectral content reveal that the spans are generally similar in response, though the natural frequencies vary slightly among the spans. This is likely due to preexisting deterioration, temperature effects, or end-fixity/bearing discrepancies, as the spans share a common design and length. A more in-depth discussion of the modal testing and the results can be found in Whelan et al. (2009).

4.2 Strain-based analysis

Load testing and rating was completed on the bridge superstructure utilizing a total of 39 BDI strain transducers deployed at the midspan, near the supports and in selected alternative sections within the north span. Two sensors directly next to each other (i.e., 2 and 3 or 20 and 30) as shown in Figure 3b indicate monitoring on the top and bottom flanges (Figure 6d) for calculating the NA location. A typical strain response at the midspan of an interior and exterior girder of the center span as well as at a bearing on the south pier of the center span is illustrated in Figure 6. It should be noted that the response in Figure 6c depicts actual strain present at the completion of the 180-second time series, indicating possible drift within the system. However, in this particular case, loading was still present on the superstructure at the end of the time history, creating a nonzero strain response. Furthermore, there are negative strains shown in the bottom flange between 40 and 80 seconds in Figures 6a

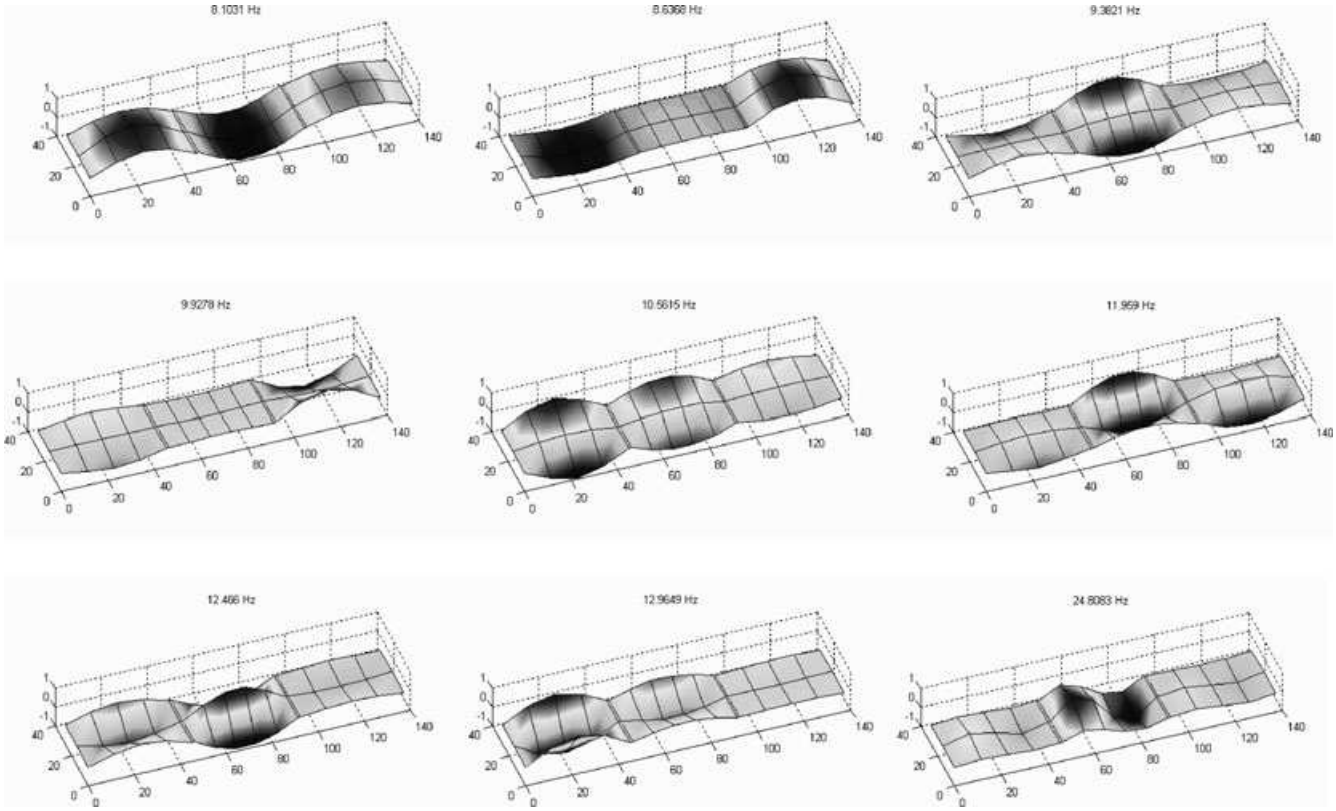

Fig. 5. Lower order mode shapes (note: 1 m = 3.28 ft).

and b from the truck leaving the north span to enter the center span. Twenty-three wireless and one wired sensor at the midspan (bottom flange of G2 on the south span) were employed for determining various section properties and demand parameters within the structure. A total of seven static (stationary) load tests were conducted using a combination of two H trucks (weighing 21.74 metric tons each) in three separate loading lanes. Initially, the entire structure is in an unloaded state. After a brief few seconds with zero strain on the bridge, the test vehicle(s) drive south along the bridge stopping for a period of approximately 20–30 seconds at the midspan of each of the three spans. In the case of one test vehicle in a particular loading lane, the rear axle is positioned at the midspan of the particular span (Figures 7a–d). When two vehicles are used in one loading lane (Figures 7e–g), the rear axles are positioned approximately 1.5 m (5 ft) on both sides of the midspan. This is the distance between the rear axle and the back of the dumper on the truck, allowing for tighter vehicle configuration within the lane. Figures 7 and 8 display the position of the test vehicles for each of the seven tests performed on each span. Figure 9 is a photo of two trucks positioned on the center lane during the load test.

4.2.1 Neutral axis locations. NA location can give engineers an indication as to the change in section stiffness at crucial locations of the superstructure. A rise or fall in its value could indicate, among other things, loss of composite action and section loss within the girder or slab, or a higher level of composite action not accounted for in design. If the NA location is too high within the slab, a larger portion of the concrete deck will be subjected to additional tensile forces which in turn will cause further cracking in the concrete and exposing reinforcement to a possible corrosive environment. Therefore, monitoring its location has a high level of importance in bridge performance monitoring. Of particular interest for this monitoring were characteristics of the structure related to the level of capacity and demand. NA locations, transverse load DF and impact factors were established within each span. All three spans were simply supported. The NA locations were computed from strain measurements at the top and bottom flanges (Figure 6d) of the girder assuming a linear strain profile along the depth of the section. The strains used for this computation resulted from the static positioning of the truck at the midspan of the span of interest. The average values and standard deviations of the measurement locations with respect to the average

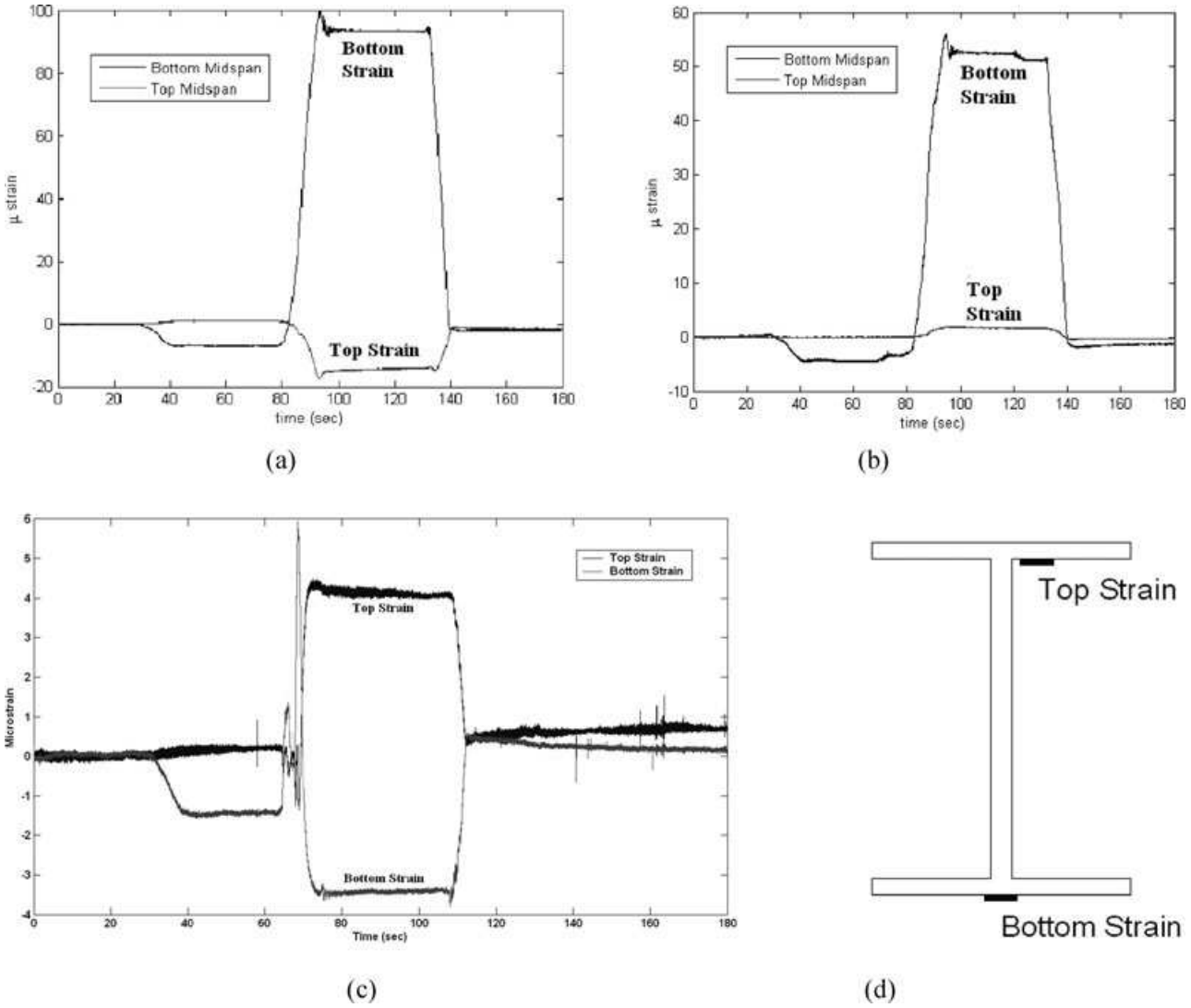

Fig. 6. Typical strain response measured: (a) at an interior girder at midspan, (b) at an exterior girder at midspan, (c) at a bearing (girder 3 south pier), and (d) strain sensor placement on top and bottom flange.

value were computed based on averaging all seven load cases as well as identical "lane loading" cases as Elhelbawey et al. (1999) suggest that values of the NA are dependent on the transverse positioning of the load and a measured value near the location of loading will produce more accurate results than a measurement far away from the load. For example, one truck in the west lane (Figure 7a) was averaged with the result from two trucks in the west lane (Figure 7e) and so on. Only one test was completed with loading in both the east and west lanes and therefore no average or standard deviation for that load case is present. The transverse positioning of the test vehicle(s) had a significant impact on the recorded wireless strain measurements at both the top and bottom flanges of the steel girder. This is clearly evident in the data presented in Tables 1–3 when the loading is farthest away from the instrumented location. At these locations, strain measurements at both the top and bottom flange were recorded between -1 and $+1$ microstrain which produced erroneous results and therefore are not presented in the tables. The quantization resolution of the ADC is approximately 0.08 microstrain with typical peak-to-peak noise around 0.2 microstrain. Such small signal-to-noise ratios preclude use of such small magnitude measurements for NA determination because the error bounds will exceed reasonable tolerances. For example, upon completing a sensitivity analysis of the data using a resolution of 0.1 microstrain, the girders for which the recorded data from both the top and bottom flanges were within the ± 1 microstrain range showed an absolute variation of

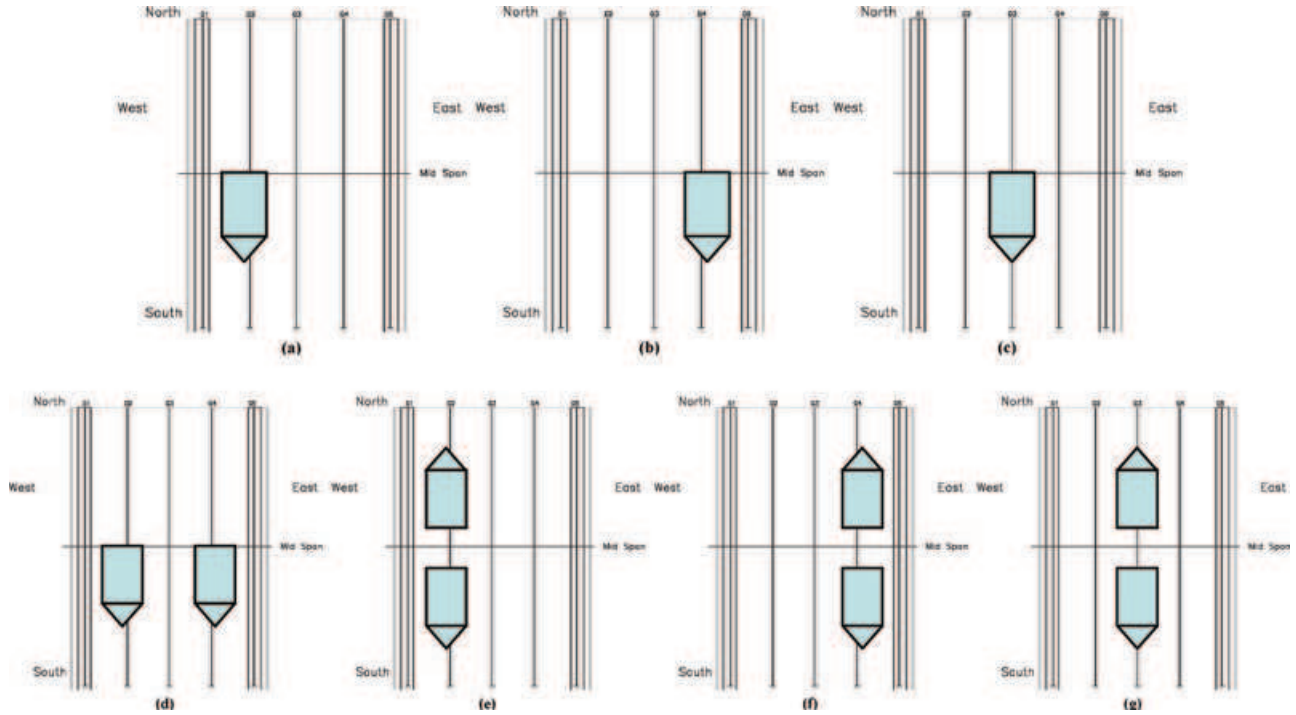

Fig. 7. Truck locations for static load testing: (a) one truck west lane, (b) one truck east lane, (c) one truck center lane, (d) one truck in east and west lane, (e) two trucks west lane, (f) two trucks east lane, and (g) two trucks center lane.

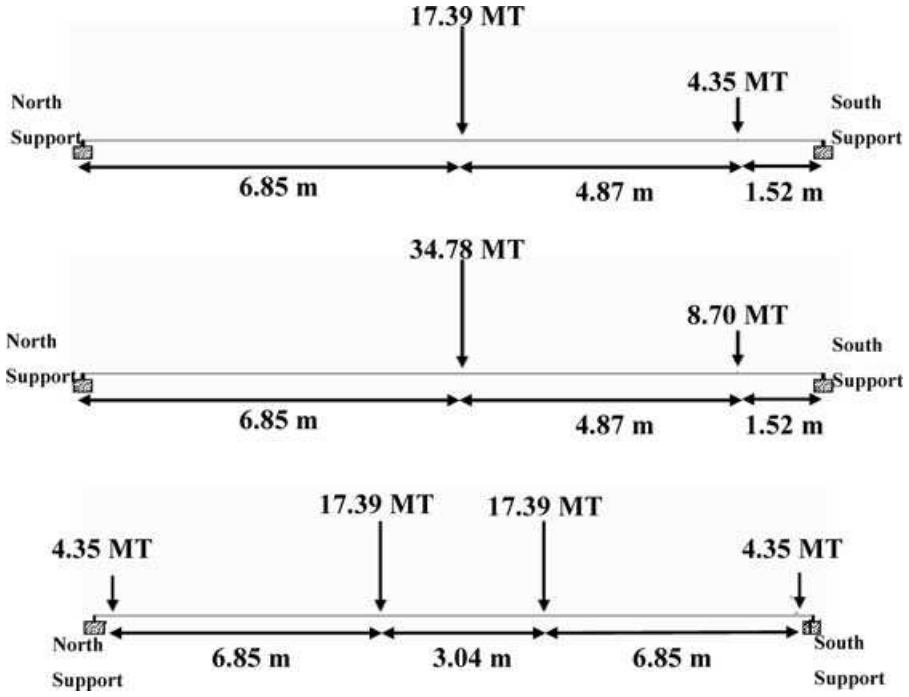

Fig. 8. Bridge elevation view of the truck loading for each of the 13.85 m (45 ft) spans based on load cases corresponding to (a) Figures 7a–c, (b) Figure 7d, and (c) Figures 7e–g (MT: metric ton).

Fig. 9. Two test vehicles in the center lane during load testing.

approximately 5.08 cm (2 in) to 86.36 cm (34 in) from the computed value. As a result, the forthcoming analysis of the NA locations for each of the three spans only relies on the following data: west lane for girders 1–3, center lane for girders 2–4, east lane for girders 3–5, and east/west lane for all girders which is presented in Table 4. These conditions produced large enough strain readings at the top and bottom flanges that under a ±0.1 microstrain change produced less than 1.27 cm (0.5 in) in absolute variation from the computed NA location based on the measured response.

As part of the original load test, strain transducers were placed at alternative locations of the north span away from the midspan along girders 1–3 (sensors 2, 3, 15, 16, 17, 18 in Figure 3b). These locations were selected based on visual differences in deterioration which may account for a varying response to the midspan measurement. The primary purpose of these measurements was to determine if the NA differed between the alternate sections and the midspan locations. Table 1 presents the results where "alternate" refers to the monitored location away from the midspan (i.e., sensors 2, 3, 15, 16, 17, 18 in Figure 3b). The results indicate a strong discrepancy among the findings at the midspan and alternate monitoring locations of girders 2 and 3. As the NA location appears to be much higher at the alternate locations, there is a possibility that the deterioration of the steel girder has caused the NA to shift toward the stiffer deck element. Alternatively, girder 1 shows a slightly better similarity between the two locations. Upon visual inspection, girder 1 appeared to possess the greatest uniformity in condition among girders 1–3 in the north span. Additionally, girders 1 and 5 show a higher NA compared to the remaining girders

Table 1
Average neutral axis (NA) locations from the base of the girder within the north span

		Girder 1 midspan	*Girder 1 "alternate"*	*Girder 2 midspan*	*Girder 2 "alternate"*	*Girder 3 midspan*	*Girder 3 "alternate"*	*Girder 5 midspan*
	Sensors	7, 8	17, 18	1, 6	15, 16	4, 5	2, 3	21, 22
West lane	Average [cm] (in)	[89.87] (35.38)	[76.97] (30.30)	[44.48] (17.51)	[67.83] (26.70)	[56.61] (22.29)	[78.98] (31.10)	–
	Standard deviation [cm] (in)	[2.567] (1.010)	[3.784] (1.490)	[1.845] (0.726)	[12.362] (4.867)	[7.861] (3.095)	[0.889] (0.350)	–
East lane	Average [cm] (in)	–	–	–	–	[50.34] (19.82)	[79.17] (31.17)	[82.45] (32.46)
	Standard deviation [cm] (in)	–	–	–	–	[4.345] (1.710)	[0.778] (0.306)	[0.815] (0.321)
Center lane	Average [cm] (in)	–	–	[65.00] (25.59)	[80.05] (31.52)	[42.54] (16.75)	[78.57] (30.93)	–
	Standard deviation [cm] (in)	–	–	[3.671] (1.445)	[1.753] (0.690)	[3.671] (1.445)	[1.598] (0.629)	–
East/west	Location [cm] (in)	[96.88] (38.14)	[82.22] (32.37)	[42.57] (16.76)	[80.62] (31.74)	[39.74] (15.64)	[79.12] (31.15)	[81.70] (32.16)
All relevant cases	Average [cm] (in)	[92.21] (36.30)	[78.72] (30.99)	[52.31] (20.59)	[75.28] (29.64)	[48.39] (19.05)	[78.94] (31.08)	[82.20] (33.07)
	Standard deviation [cm] (in)	[4.43] (1.75)	[4.04] (1.59)	[11.66] (4.59)	[9.23] (3.63)	[7.960] (3.134)	[0.853] (0.336)	[0.72] (0.28)

Note: Depth of girders 1 and 5 is 13.11 cm (33.3 in) and depth of girders 2 and 3 is 13.19 cm (33.5 in).

Table 2
Neutral axis (NA) measurements (from the bottom flange) within the center span

		Girder 1 midspan	*Girder 3 midspan*	*Girder 5 midspan*
	Sensors	9, 10	12, 13	23, 24
West lane	Average [cm] (in)	[84.11] (33.11)	[77.02] (30.33)	–
	Standard deviation [cm] (in)	[0.0342] (0.0134)	[2.299] (0.9051)	–
East lane	Average [cm] (in)	–	[74.16] (29.20)	[92.64] (36.48)
	Standard deviation [cm] (in)	–	[1.902] (0.7488)	[1.780] (0.7007)
Center lane	Average [cm] (in)	–	[74.04] (29.15)	–
	Standard deviation [cm] (in)	–	[2.432] (0.9574)	–
East/west	Location [cm] (in)	[84.92] (33.43)	[72.00] (28.35)	[98.71] (38.86)
All relevant cases	Average [cm] (in)	[84.38] (33.22)	[74.64] (29.39)	[93.44] (36.79)
	Standard deviation [cm] (in)	[0.47] (0.18)	[2.39] (0.94)	[3.72] (1.46)

Note: Depth of girders 1 and 5 is 13.11 cm (33.3 in) and depth of girder 3 is 13.19 cm (33.5 in).

Table 3
Neutral axis (NA) measurements (from the bottom flange) within the south span

		Girder 1 midspan	*Girder 3 midspan*	*Girder 5 midspan*
	Sensors	14, 19	20, 30	25, 26
West lane	Location [cm] (in)	[87.92] (34.61)	[72.14] (28.40)	–
	Standard deviation [cm] (in)	N/A	N/A	–
East lane	Average [cm] (in)	–	[70.33] (27.69)	[87.74] (34.54)
	Standard deviation [cm] (in)	–	[3.154] (1.242)	[0.4328] (0.1704)
Center lane	Average [cm] (in)	–	[56.33] (22.18)	–
	Standard deviation [cm] (in)	–	[3.455] (1.360)	–
East/west	Location [cm] (in)	[92.01] (36.22)	[57.45] (22.62)	[89.79] (35.35)
All relevant cases	Average [cm] (in)	[89.96] (35.42)	[63.82] (25.13)	[88.42] (34.81)
	Standard deviation [cm] (in)	[2.89] (1.14)	[8.110] (3.193)	[1.22] (0.48)

Note: Depth of girders 1 and 5 is 13.11 cm (33.3 in) and depth of girder 3 is 13.19 cm (33.5 in).

Table 4
Average neutral axis (NA) locations and 95% confidence interval (CI) of the mean (measurements referenced from the bottom flange of the girder)

		Mean [cm] (in)	*Standard deviation [cm] (in)*	*Lower 95% CI [cm] (in)*	*Upper 95% CI [cm] (in)*
North span	Girder 1 (G1)	[92.21] (36.30)	[4.43] (1.75)	[81.19] (31.97)	[103.2] (40.64)
	Girder 2 (G2)	[52.31] (20.59)	[11.66] (4.59)	[37.83] (14.86)	[66.77] (26.29)
	Girder 3 (G3)	[48.39] (19.05)	[7.96] (3.13)	[41.02] (16.15)	[55.75] (21.95)
	Girder 5 (G5)	[82.20] (33.07)	[0.72] (0.28)	[80.40] (31.65)	[84.00] (33.07)
Center span	Girder 1 (G1)	[84.38] (33.22)	[0.47] (0.18)	[83.21] (32.76)	[85.54] (33.68)
	Girder 3 (G3)	[74.64] (29.39)	[2.39] (0.94)	[72.43] (28.51)	[76.85] (30.26)
	Girder 5 (G5)	[103.9] (40.91)	[3.72] (1.46)	[85.42] (33.63)	[103.9] (40.91)
South span	Girder 1 (G1)	[89.96] (35.42)	[2.89] (1.14)	[63.97] (25.18)	[116.0] (45.65)
	Girder 3 (G3)	[63.82] (25.13)	[8.11] (3.19)	[55.31] (21.78)	[72.33] (28.48)
	Girder 5 (G5)	[88.42] (34.81)	[1.22] (0.48)	[85.39] (33.62)	[91.46] (36.01)

Note: Depth of girders 1 and 5 is 13.11 cm (33.3 in) and depth of girder 3 is 13.19 cm (33.5 in).

at midspan likely due to the 20.32 cm (8 in) curb on the exterior of each side of the bridge. This along with deterioration of the steel girder is likely the result of the significantly higher NA location compared to the interior girders. The exterior girders are more exposed to the harsh environment and runoff from the bridge deck resulting in greater deterioration than the interior girders.

Results for the center span show fairly dissimilar results when compared to data gathered for the north span. It is apparent from Table 2 that in comparison to

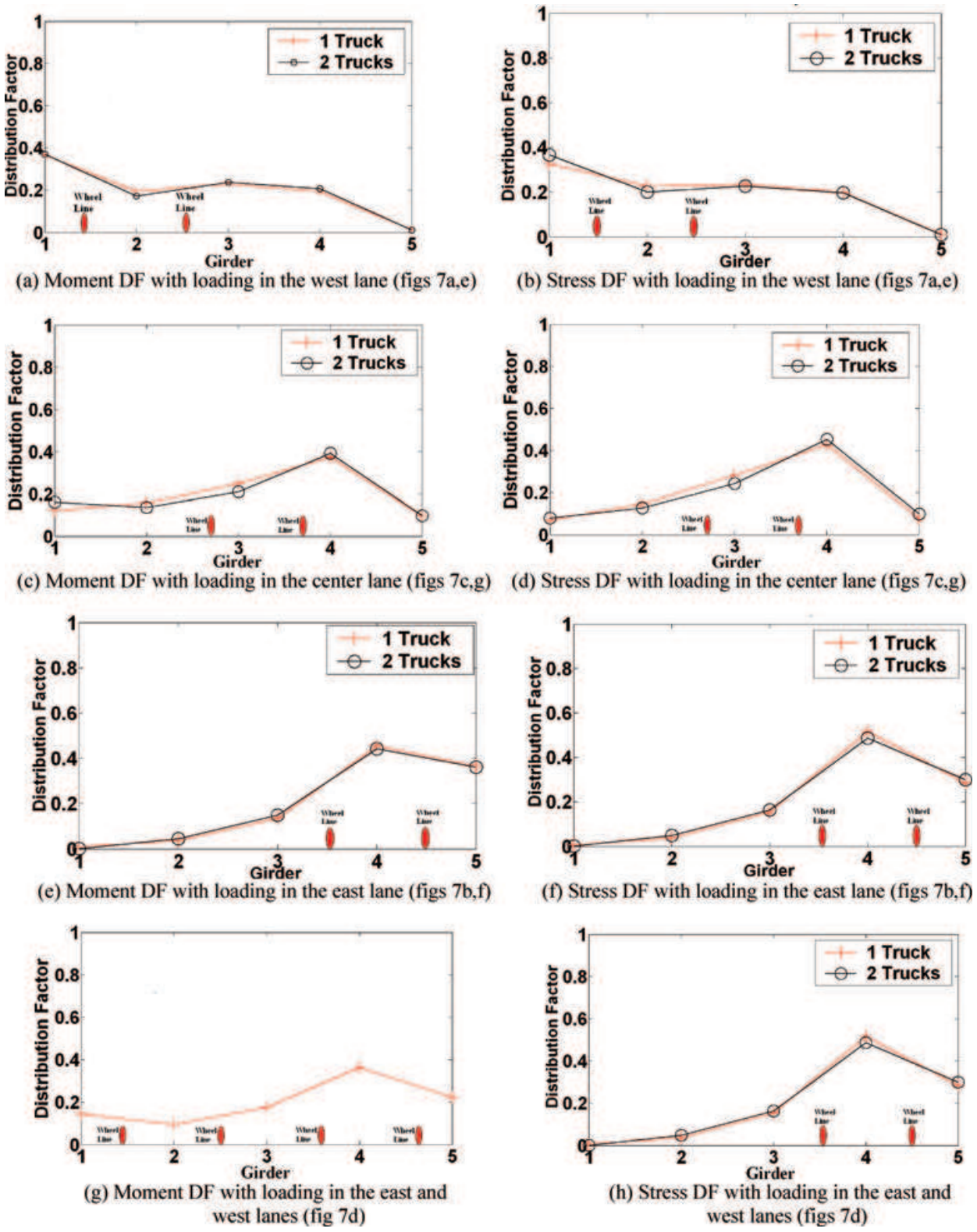

Fig. 10. A north span comparison of distribution factors (DF) with loading of one and two test vehicles in a given lane.

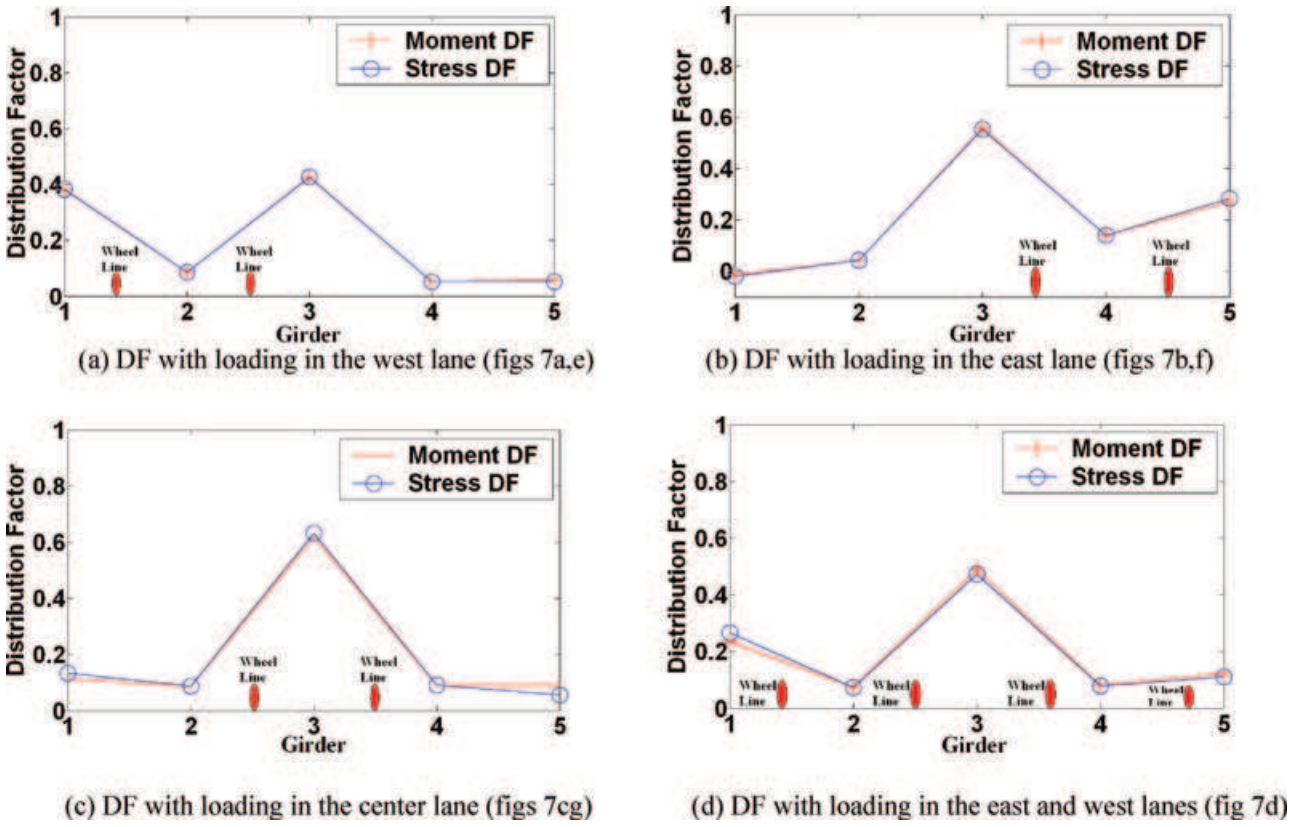

Fig. 11. Distribution factors (DF) for the center span.

the north span, the average location of the NA appears to be lower for girder 1 and higher for girders 3 and 5 with lower deviation in the measurements. A lower NA for girder 1 can indicate a less deteriorated steel girder compared to the north span or less composite action between the bridge deck and girder. Upon visual inspection, girder 1 of the center span appeared less deteriorated than girder 1 of the north span. The opposite findings in the data are suggested for girder 3 and 5. In most cases, the NA appears to be located somewhere between the top flange of the girder and the lower portion of the reinforced concrete deck. There were two load cases within girder 5 which caused significantly erroneous results. As seen in Table 2, truck loading in the west and center lanes produced large deviations among the data in addition to NA locations outside the depth of the concrete slab/steel girder section. These inconsistencies are likely the result of small strain measurements in the top and/or bottom flange which can produce errors and large deviations in the results due to the sensor resolution as discussed previously. These small strains can be seen from the transverse load distribution plots (to be discussed later), in particular Figures 10e, f and 12a, b. Much larger strain readings are present with in girders with which the loading is directly over or in the vicinity of the girder resulting in much lower deviation in the measured locations. Again, the NA locations of the exterior girders were typically higher than the interior girders likely due to the higher edge stiffness from the curbs as well as deterioration of the steel girder.

The south span of the bridge had a similar sensor layout to the center span with strain transducers placed at the top and bottom flanges at midspan of the two exterior and center girders. Table 3 displays the results from the completed load tests. Unlike the previous two spans, a back to back truck configuration in the west lane (Figure 7e) could not be completed due to the positioning of the test center data acquisition vehicle. As a result, only one point was used in determining an average NA location in the west lane load cases and subsequently no standard deviation is computed. In contrast to other spans, the locations of the NA appear to be similar for girders 1 and 5 when the test vehicle is positioned over the particular girder. For example, girder 1 under west lane loading is similar to girder 5 under east lane loading. Girder 3 under symmetric loading (i.e., center and east/west lanes) displayed nearly identical results.

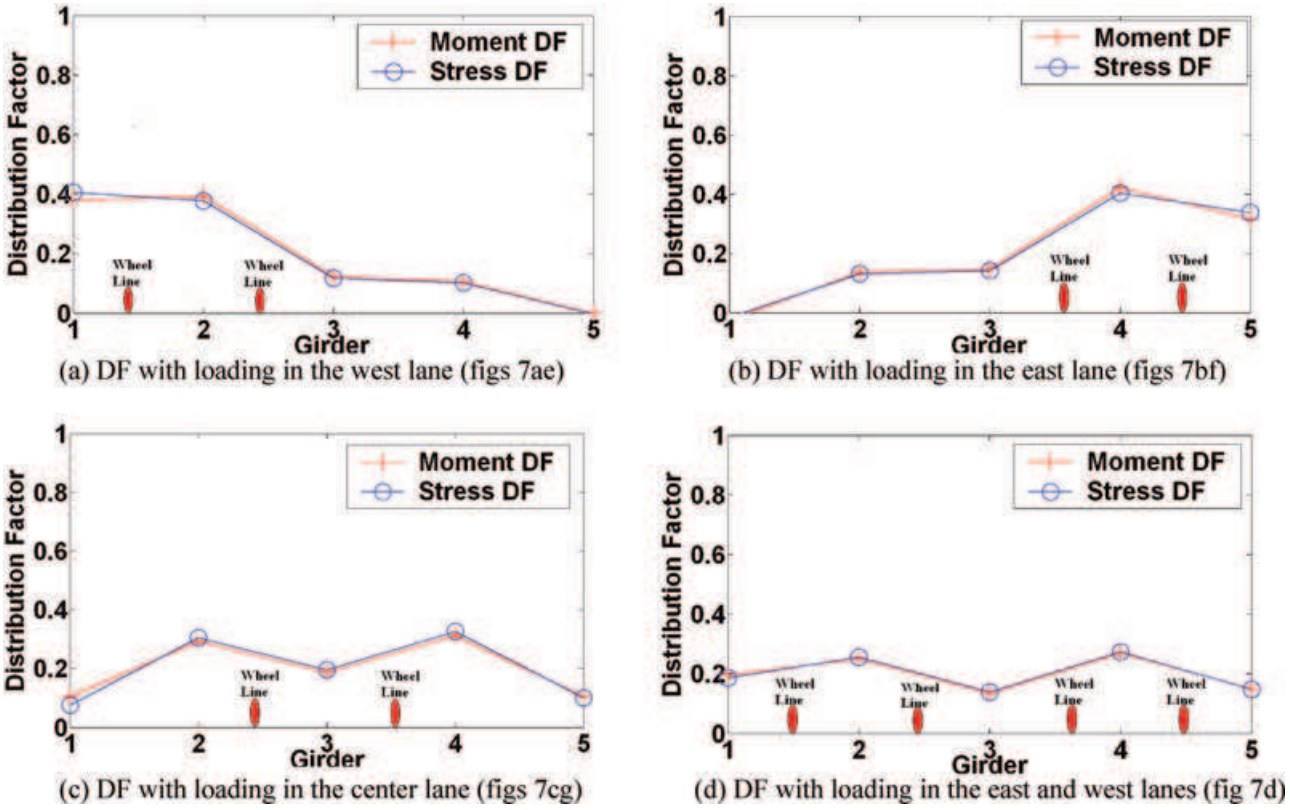

Fig. 12. Distribution factors (DF) for the south span.

Table 4 highlights the average NA value at the midspan of each instrumented girder taken from load tests on each of the three spans. The averaging results are based on the loading criteria mentioned previously: west lane for girders 1–3, center lane for girders 2–4, east lane for girders 3–5, and east/west lane for all girders. Each span is nearly identical in design which would suggest results should be nearly similar for all spans. However, due to the deterioration and differing material properties at different locations of the structure, results will vary. An upper and lower 95% confidence interval (CI) on the mean NA location was computed for the center and two exterior girders of each span. Elhelbawey et al. (1999) determined that the NA locations are normally distributed. Therefore, a *t*-distribution was selected as the data set was small and extra variability in the standard variable based on the sample standard deviation is expected. The confidence intervals were therefore generated based on the sample average, standard deviation, number of samples, and appropriate *t*-critical value. It is noted that each of the upper and lower bounds in the CI are located within the depth girder/slab section. A large confidence band is shown for girder 1 of the south span on account of the number of points used in the averaging process. As a back to back configuration of the test trucks in the west lane (Figure 7e) could not be achieved on this span due to reasons discussed earlier, only two points were used in the averaging and therefore a much higher *t*-critical value was used for greater uncertainty. Furthermore, the NA location within girder 3 lies within the steel girder in each span although the exterior girders are heavily influenced by the reinforced concrete curb and deterioration of the steel girder due to harsher exposure to climate conditions and bridge deck runoff.

4.2.2 Distribution factors. Load DF are a measure of load transfer through the structure. As a means of safety, the load is typically shed to other bridge elements as to not overstress the primary load carrying member. For this to occur, the load is transferred transversely within the structure through the bridge deck and diaphragms. Each of the three spans' strain transducers were placed on the bottom flange at midspan of each girder of all three spans. This measurement was combined with the section modulus computed from the top strain transducers at the exterior and center girders to calculate the bending moment. To compute the section

modulus, an effective flange width was calculated from composite section analysis combined with the NA results obtained previously. The moment distribution factor was therefore computed from Equation (1) where M_i is the bending moment of girder i, S_x is the section modulus, E is the elastic modulus, and ε is the bending strain. As the center girder was the only interior girder monitored for NA location, the analysis assumed that the remaining two interior girders possess the same section modulus:

$$DF_i = \frac{M_i}{\sum M_i} = \frac{S_{x,i} E_i \varepsilon_i}{\sum S_{x,i} E_i \varepsilon_i} \quad (1)$$

Loads were positioned in the three different lanes to maximize the response to the structure; creating the most critical load cases. Loading isolated at one particular location of the structure produces a greater distribution factor response compared to loading spread along the width of the bridge (i.e., loading in two separate lanes). Data displayed in Figure 10 show that the transverse positioning of the loading has a greater effect than the actual load within a particular lane. This is evident from the transverse load distribution behavior depicted within Figure 10 with one and two trucks loaded in a particular loading lane. Results from the center and south spans produced similar findings which are not displayed in this article to conserve space. Based on this information, an average value of the distribution factor for each loading lane was used in the remaining analysis.

The results illustrate that, for the most part, a higher distribution factor is present near the loading locations. This is not seen in the center lane load case (Figures 10c and d) as a majority of the demand is placed on girder 4 instead of girder 3 where the load is concentrated. Nevertheless, it is interesting to note that a mirror image is not seen when contrasting the east lane to west lane load cases. This is likely due to deterioration within the superstructure; particularly in the west side (girders 1 and 2) as there is a lower distribution factor for girder 2 compared to girders 3 and 4 when there is loading in the west lane. Additionally, the position of the test vehicle may not have been exactly mirrored which would alter the results. However, this is likely not the case as the test vehicles were positioned at premarked locations. Another possible error could be in assuming the section properties (i.e., section modulus) of girder 4 were identical to girder 3. If this were not the case, the remaining values would be misrepresented. It is often necessary to make these assumptions however due to lack of instrumentation for monitoring every girder. A single faulty sensor reading would also produce inaccurate results as the DF for each girder is dependent on each of the other girders. If additional time were available to complete the testing, repeated tests would have been completed to provide adequate statistical analysis.

The stress DF were computed in addition to the moment DF on account of select cases where the section modulus was determined to be suspect. This is expected based on the data presented earlier of the NA locations. When comparing the differences of both the stress and moment-based methods, the results appear to be very similar. The greatest dissimilarity among the results appears to be in Figures 10c and d within girder 1 likely due to the higher deviation in the data for girder 1 as shown in Table 1. Additionally, the data show that the load distribution to the exterior girder farthest from the loading (i.e., girder 1 with loading in the east lane and girder 5 with loading in the west lane) is not very high. This small strain impacted select cases of the NA measurements as discussed previously. In all cases, the moment and stress-based method shows approximately a 45% maximum load carried by one girder. This is approximately equivalent to the design value of the exterior girders (43%) but well below the interior design value (62%) based on American Association of State Highway and Transportation Officials (AASHTO) Standard Bridge Design Specifications (2002).

Although one would not expect the stress and moment-based DF values to exactly match due to differing section moduli, the trends and relative closeness should be apparent. The north span displayed some discrepancy among the two methods which is much less apparent for the center span as seen in Figure 11. In the first two cases (Figures 11a and b) there is very little if any significant difference. There are however some anomalies present within the various distributions that were not expected. Loading in either the east or west lane (Figures 11a and b) shows a higher distribution of the loading to the center girder as opposed to the girder where the load is concentrated. Girders 1 and 5 are not demanding a high concentration of the load when the truck is in the east and west lanes respectively. The presence of the curb and deck overhang typically results in a stiffer section than an interior girder and therefore has a greater load demand. This result could suggest some internal damage to the structure in transferring the loading to selected members. It is evident from the loading locations that girders 2 and 4 are not demanding the load that one would expect. This could be the result of poor sensor readings or damage within the bridge elements which in turn alters the results for the remaining girders. A maximum distribution of approximately 62% is observed when loading occurs in the center lane. Although testing in the north span did not show any mirrored responses from the east lane and west lane load cases, there appears to be a much closer response here.

Furthermore, it is observed that a numerical average of the east lane and west lane load cases produce results similar to that found in Figure 10d. In each load case there is heavy bias towards the center lane girder.

The south span showed distinctly differing results from the other two spans. The load case corresponding to loading in the east lane (Figure 12b), shows the primary load carrying member to be the girder which the truck is directly over (girder 4). A near reflective pattern is seen with loading in the west lane over girder 2. It is interesting to note that the distribution of the loading to girder 3 in Figures 12c and d is lower than that of girders 2 and 4 when the load is directly atop of girder 3. Both results could suggest that the stiffness of the center girder is not as great as the remaining two interior girders. A comparison between the stress-based and moment-based DF values appear to correlate strongly, similar to that of the center span. In comparison to the remaining two spans, only loading in the east lane (Figure 12b) is similar to identical load case in the center span (Figure 11b).

Figures 10–12 display different behaviors based on identical loading conditions of three very similarly designed spans. The existence of damage or change in section properties within each of the spans likely explains the difference in results. One such example of this damage is the presence of a restraint bearing of girder 3 in the center span; this is clearly depicted from the strain time history in Figure 6c. Ideally, an expansion bearing would allow for free rotation and longitudinal translation. However, the presence of negative strain in the bottom flange indicates rotational restraint exists. In fact, the most recent biennial inspection report noted overextended bearings and that "corrosion on the rocker bearing interface and upper socket assembly restrict its free movement," thereby suggesting the presence of significant, and most probably nonuniform, fixity at malfunctioning bearings. An example of a pinned bearing with significant corrosion on the northern pier for girder 5 is shown in Figure 13. Furthermore, according to tilt sketches taken at -1°C and subsequently at 28°C, the bearing inspected in the routine was found to experience virtually no movement despite the large temperature differential implying a fixed condition caused by corrosion and packing. A nonuniform change in bearing restraint across the different girders is a probable cause of the unanticipated differing responses recorded. These results suggest that the response of the as-built structure has changed as identical loading cases on nearly identical span layouts in a healthy structure should produce a similar behavior. Unlike in the case of the NA locations, the resolution and quantization of the noise of the strain measurement did not play as significant a role in the DF result. This

Fig. 13. Corroded bearings at the northern-most pier of the bridge.

is due to the fact that the total flexural strain/moment at midspan (i.e., $\sum S_{x,i} E_i \varepsilon_i$) is much larger and dominates the individual strain/moment of any one girder ($S_{x,i} E_i \varepsilon_{\mathrm{i}}$). A $\pm$ 0.1 microstrain difference in the strain reading produces less than a 2% absolute difference from the calculated DF based on the acquired strains.

4.2.3 Dynamic allowance. Dynamic allowance (DA), or impact factor, is a measure of the stress state beyond static conditions and when used in design helps to control excess vibrations from vehicle loads. Tests were run at various speeds ranging from a semi-static crawl speed (8 km/h or 5 mph) to dynamic speeds of 72.4 km/h (45 mph) with the test truck driving down the center lane of the bridge from north to south. The DA is computed in Equation (2) where $\varepsilon_{\mathrm{semi-static}}$ refers to the strain measurement when the vehicle is traveling at 8 km/h (i.e., baseline speed) and $\varepsilon_{\mathrm{dyn}}$ is the dynamic strain at speeds above 8 km/h. As displayed in the results presented in Figure 14, there appear to be select cases where the impact factor is negative or unreasonably high, particularly in the north and south spans. The direction of the test runs (north to south) could be the reason for the higher impact factors on the north span compared to the south as the condition of the approaches influence the impact factor. Test runs from south to north would therefore likely produce different results. Even so, all data are presented to show the results captured during the tests. Typically, the stresses within the girders increase until an optimum speed is reached then decreases; the results in this case appear random. As road roughness and vehicle dynamics can alter the effects of the impact stresses, the select cases of improbable results are partially explained by these consequences. The results from the center span appear most typical with an

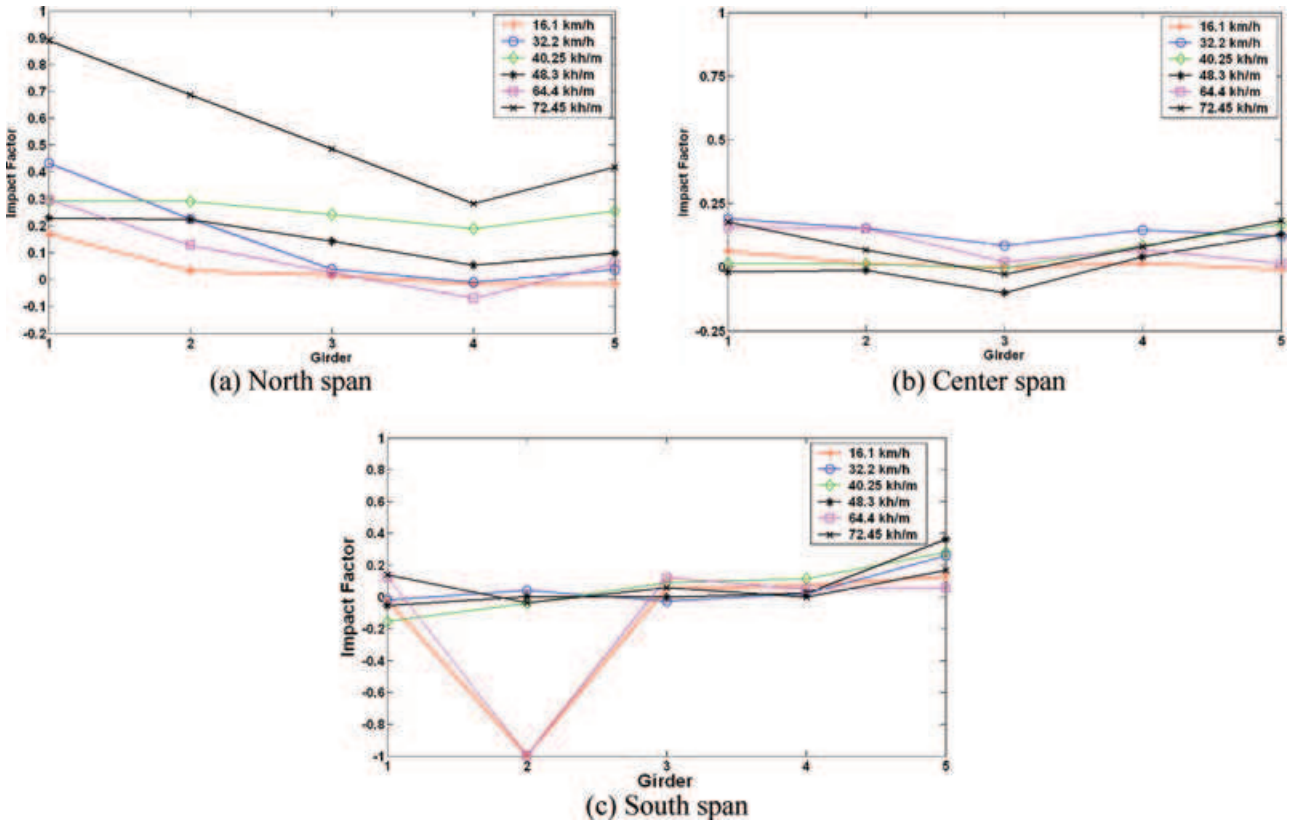

Fig. 14. Impact factor response for each of the three spans.

approximate impact factor of about 0.2. It seems that in all cases, the maximum values are within the exterior girders. These maximums within the north and south spans appear to be greater than the AASHTO (AASHTO, 2002) design value of 0.294. This is an indication that the design moment amplification for dynamic impact response is greater than the in situ conditions of the span:

$$DA = \frac{\varepsilon_{dyn} - \varepsilon_{semi-static}}{\varepsilon_{semi-static}} \tag{2}$$

4.2.4 Load rating analysis. Data obtained from the NA locations, DF, and dynamic allowance factors were subsequently used to complete a load rating of the superstructure. The rating factor (RF) was determined using the AASHTO Manual for Condition Evaluation of Bridges (AASHTO, 2001) based on flexure as the rating limit state. Equation (3) provides the RF based on working stress method where C is the capacity of the member, S_x^{LL} is the live load section modulus determined from the previous NA computations, S_x^{DL} is the dead load section modulus, S_x^{SDL} is the superimposed dead load section modulus, M_{LL} is the live load moment, and I is the maximum impact factor. Figures 14a and c indicate a maximum impact factor greater than the maximum specified value from AASHTO of 0.3. Therefore, 0.3 was used in place of the maximum values displayed in the results. Dead loads were contributed from the steel girders, diaphragms, and bridge deck although the superimposed dead loads were from the curb, railings, and asphalt wear surface. The section properties and moment demands in both cases were computed from the as-built structural drawings of the bridge:

$$\mathrm{RF} = \frac{CS_x^{LL} - M_{DL}\dfrac{S_x^{LL}}{S_x^{DL}} - M_{SDL}\dfrac{S_x^{LL}}{S_x^{SDL}}}{M_{LL}(1+I)} \tag{3}$$

The RF were calculated from both an AASHTO rating ($\mathrm{RF_{AASHTO}}$) (theoretical) as well as from test-based results ($\mathrm{RF_{Test}}$) for inventory and operating loading levels and are presented in Tables 5 and 6 respectively. Inventory loading corresponds to design stresses and current material conditions, such as deterioration and loss of section. A live load at this level can be applied to the existing structure for an indefinite period of time. Operating load level is "the

Table 5
Inventory rating factors (RF) for each span

Span	RF_{AASHTO}	RF_{Test}
North	1.15	1.35
Center	1.47	1.58
South	1.33	2.16

Table 6
Operating rating factors (RF) for each span

Span	RF_{AASHTO}	RF_{Test}
North	1.87	2.19
Center	2.38	2.56
South	2.16	3.06

maximum allowable live load the structure can withstand. Too much use at operating level reduce the service life of the structure" (AASHTO, 2001). The AASHTO rating incorporated specified values (DF and I) from the AASHTO Bridge Design Specification Manual (AASHTO, 2002) as well as from the AASHTO Manual for Condition Evaluation of Bridges (AASHTO, 2001) for live load parameters although the live load section modulus (S_x^{LL}) was taken to be the average value corresponding to the tests used to compute the NA locations in Table 4. The test-based RF employed data pertaining to the demand on the structure (DF and I) from the load test although the AASHTO live load moment from the rating manual based on the 21.75 metric ton test vehicle was used for the live load moment (M_{LL}). A RF was calculated for the exterior girders as well as interior girders and the smallest value is considered the RF for the span.

Upon analyzing the load testing data for each of the three spans, it appears that the inventory RFs are all above the safe level based on a weight of 21.75 metric tons. Multiplying the RF by the truck weight (21.75 metric tons) produced the load rating of the span. The inventory RF for the entire superstructure based on the test-based data is 1.35 or 29.36 metric tons.

5 CONCLUSION

A WSS developed at Clarkson University was deployed on a three-span simply supported bridge in New York State. The study focused on capturing both the modal and strain-based characteristics of the superstructure. A total of 90 wireless accelerometers and strain transducers along with an additional 9 wired strain transducers were installed with readings taken over a 2-day testing period. Nine wired sensors were required as only 30 wireless nodes were available for testing. All measurements were sampled at an effective rate of 128 Hz in real time through two simultaneously operating star topology networks. Operational modal analysis revealed that the first-order natural frequencies of the spans were generally in the range of 8 Hz to 13 Hz. The first nine lower order mode shapes of the entire superstructure are presented as extracted from stochastic subspace identification. Strain measurements provided NA locations at the midspan of the center and two exterior girders of each of the three spans along with specific "alternate" locations away from the midspan on three girders of the north span. Additionally, impact factors were computed for different passing speeds of the test vehicles. Maximum values in the north and south spans were above the AASHTO design and rating values. Moment DF computed at the midspan of each girder suggest load transfer throughout the superstructure. There did however appear to be certain anomalies among specific data within the center and south span based on the loading conditions, possibly due to frozen rocker bearings, structural deterioration, or changes in material or geometric properties among the spans. Most notably, the presence of bearing restraint at the rocker bearings indicates unanticipated levels of end fixity, likely due to the severe corrosion that is corroborated through visual inspection reports. Additionally, low strain readings in the top and bottom flanges resulted in some high deviation among NA measurements. A sensitivity analysis performed based on the resolution and quantization of the noise of the strain readings from the wireless system suggests large deviation from the calculated NA location when both top and bottom strains are recorded to be within ± 1 microstrain. Due to a lack of time for testing, repeated tests were not completed at a particular loading location. Multiple tests would allow for more accurately verifying the results. A load rating of 29.36 metric tons was computed based on the flexure rating state using the data set gathered. To the knowledge of the authors, this is the first wireless load rating completed in the state of New York and is the first full load rating completed using the WSS. Shortly upon completing the load testing, controlled progressive damage was implemented to the superstructure to test the capability of detecting damage from various algorithms. Information pertaining to the damage detection based on global acceleration measurements can be found in Whelan and Janoyan (2010). This deployment demonstrates the capability of the developed wireless sensor network to address load testing and rating on an expedited and efficient schedule.

ACKNOWLEDGMENTS

The authors would like to acknowledge the New York State Department of Transportation and, in particular, the Region 7 engineers and bridge maintenance crew for facilitating and assisting with the field testing. Additionally, the authors also wish to thank Professor Ratneshwar Jha and graduate students, Wei Chen and Jessica Rocheleau, and undergraduate students, Francis Dayamba and Sarah Marin, for their on-site assistance during the sensor installation.

REFERENCES

Adeli, H. & Jiang, X. (2006), Dynamic fuzzy wavelet neural network model for structural system identification, *Journal of Structural Engineering, ASCE*, **132**(1), 102–11.

American Association for State and Highway Transportation Officials (AASHTO), (2001), *Manual for Condition Evaluation of Bridges*, American Association for State and Highway Transportation Officials, Washington DC.

American Association for State and Highway Transportation Officials (AASHTO), (2002), *Standard Specifications for Bridge Design*, American Association for State and Highway Transportation Officials, Washington DC.

Bridge Diagnostics Incorporated (BDI), (2008), Wireless structural testing system (STS-WiFi). Available at: http://www.bridgetest.com/products/bdi_sts-wireless.html, accessed September 21, 2009.

Chajes, M. J., Mertz, D. R. & Commander, B. (1997), Experimental load rating of a posted bridge, *ASCE Journal of Bridge Engineering*, **2**(1), 1–10.

Chakraborty, S. & DeWolf, J. T. (2006), Development and implementation of a continuous strain monitoring system on a mult-girder composite steel bridge, *ASCE Journal of Bridge Engineering*, **11**(6), 753–62.

Chen, B. & Liu, W. (2010), Mobile agent computing paradigm for building a flexible structural health monitoring sensor network, *Computer-Aided Civil and Infrastructure Engineering*, **25**(7), 504–516.

Cruz, P. J. S. & Salgado, R. (2009), Performance of vibration-based damage detection methods in bridges, *Computer-Aided Civil and Infrastructure Engineering*, **24**(1), 62–79.

DeWolf, J. T., D'Attilio, P. F., Feldblum, E. G. & Lauzon, R. G. (2006), *Bridge Monitoring Network—Installation and Operation*, Report No. CT-2217-F-06-10. Connecticut Department of Transportation.

Doebling, S., Farrar, C., Prime, M. & Shevits, D. (1996), *Damage Identification and Health Monitoring of Structural and Mechanical Systems from Changes in Their Vibration Characteristics: A Literature Review*, Los Alamos National Laboratory Report, No. LA-13070-MA, Los Alamos, NM.

Elhelbawey, M., Fu, C. C., Sahin, M. A. & Schelling, D. R. (1999), Determination of slab participation from weigh-in-motion bridge testing, *ASCE, Journal of Bridge Engineering*, **4**(3), 165–73.

Federal Highway Administration (FHWA), (2009), Deficient bridges by state and highway system. Available at: http://www.fhwa.dot.gov/bridge/deficient.cfm., accessed February 26, 2010.

Gangone, M. V., Whelan, M. J. & Janoyan, K. D. (2009), Deployment of a dense hybrid wireless sensing system for bridge assessment, *Structure and Infrastructure Engineering: Maintenance, Management, Life-Cycle Design and Performance*, Taylor & Francis, DOI: 10.1080/15732470802670842.

Hag-Elsafi, O. & Kunin, J. (2006), *Load Testing for BridgeRating: Route 22 Over Swamp River*, Special Report New York State Department of Transportation (NYSDOT).

He, X., Moaveni, B., Conte, J. P. & Elgamal, A. (2008), Modal identification study of Vincent Thomas Bridge using simulated wind-induced ambient vibration data, *Computer-Aided Civil and Infrastructure Engineering*, **5**(23), 373–88.

Hsieh, K. H., Halling, M. W. & Barr, P. J. (2006), Overview of vibrational structural health monitoring with representative case studies, *ASCE Journal of Bridge Engineering*, **11**(6), 707–15.

Howell, D. A. & Shenton III, H. W. (2006), System for in-service strain monitoring of ordinary bridges, *ASCE Journal of Bridge Engineering*, **11**(6), 673–80.

Huang, C. S., Huang, S. L., Su, W. C. & Wu, C. L. (2009), Identification of time-variant modal parameters using TVARX and low-order polynomial function, *Computer-Aided Civil and Infrastructure Engineering*, **24**(7), 470–91.

Huang, R. Y., Mao, I. S. & Lee, H. K. (2010), Exploring the deterioration factors of bridges: a rough set theory approach, *Computer-Aided Civil and Infrastructure Engineering* **25**(7), 517–29.

Humar, J., Bagchi, A. & Xu, H. (2006), Performance of vibration-based techniques for the identification of structural damage, *SAGE Journal of Structural Health Monitoring*, **5**(3), 215–27.

Jang, S. A., Sim, S. H. & Spencer Jr., B. F. (2008), Structural damage detection using static strain data, in *Proceeding of the SMSST'07*.

Jáuregui, D. V. & Barr, P. J. (2004), Nondestructive evaluation of the I-40 bridge over the Rio Grande River, *ASCE Journal of Performance of Constructed Facilities*, **18**(4), 195–204.

Jiang, X. & Adeli, H. (2005), Dynamic wavelet neural network for nonlinear identification of highrise buildings, *Computer-Aided Civil and Infrastructure Engineering*, **20**(5), 316–30.

Jiang, X. & Adeli, H. (2008a), Dynamic fuzzy wavelet neuroemulator for nonlinear control of irregular highrise building structures, *International Journal for Numerical Methods in Engineering*, **74**(7), 1045–66.

Jiang, X. & Adeli, H. (2008b), Neuro-genetic algorithm for nonlinear active control of highrise buildings, *International Journal for Numerical Methods in Engineering*, **75**(7), 770–86.

Jiang, X., Mahadevan, S. & Adeli, H. (2007), Bayesian wavelet packet denoising for structural system identification, *Structural Control and Health Monitoring*, **2**(14), 333–56.

Lynch, J. P., Wang, Y., Loh, K. J., Yi, J-H. & Yun, C-B. (2006), Performance monitoring of the Geumdang Bridge using a dense network of high-resolution wireless sensors, *Smart Materials and Structures*, Institute of Physics Publishing, UK, **15**(2006), pp. 1561–75.

Moaveni, B., Conte, J. P. & Hemez, F. M. (2009), Uncertainty and sensitivity analysis of damage identification results obtained using finite element model updating, *Computer-Aided Civil and Infrastructure Engineering*, **24**(5), 320–34.

New York State Department of Transportation (NYSDOT). (2010), R-posted bridge limitations. Available at:

https://www.nysdot.gov/gisapps/posted-bridges/r-posted-bridge-limitation.

Park, H. S., Lee, H. M., Adeli, H. & Lee, I. (2007), A new approach for health monitoring of structures: terrestrial laser scanning, *Computer-Aided Civil and Infrastructure Engineering*, **22**(1), 19–30.

Phares, B. M., Rolander, D. D., Graybeal, B. A. & Washer, G. A. (2001), Reliability of visual bridge inspection, *Public Roads*, **64**(5), March/April.

Shenton III, H. W. & Chajes, M. J. (1999), Long-term health monitoring of an advanced polymer composite bridge, *SPIE Smart Structures and Bridges*, **3671**, 143–51.

Sohn, H., Farrar, C. R., Hemez, F. M., Shunk, D. D., Stinemates, D. W. & Nadler, B. R. (2003), *A Review of Structural Health Monitoring Literature: 1996–2001*, Los Alamos National Laboratory Report, LA-13976-MS.

Soyoz, S. & Feng, M. Q. (2009), Long-term monitoring and identification of bridge structural parameters, *Computer-Aided Civil and Infrastructure Engineering*, **2**(24), 82–92.

Umesha, P. K., Ravichandran, R. & Sivasubramanian K. (2009), Crack detection and quantification in beams using wavelets, *Computer-Aided Civil and Infrastructure Engineering*, **24**(8), 593–607.

Whelan, M. J., Gangone, M. V., Janoyan, K. D. & Jha, R. (2010), Operational modal analysis of a multi-span skew bridge using real-time wireless sensor networks, *Sage Journals, Journal of Vibration and Control*, DOI: 10.1177/1077546310373058.

Whelan, M. J., Gangone, M. V. & Janoyan, K. D. (2009), Highway bridge assessment using an adaptive real-time wireless sensor network, *IEEE Sensors*, **9**(11), 1450–13.

Whelan, M. J. & Janoyan, K. D. (2009), Design of a robust, high-rate wireless sensor network for static and dynamic structural health monitoring, *Sage Journals, Journal of Intelligent Material Systems and Structures*, **20**(7), 849–64.

Whelan, M. J. & Janoyan, K. D. (2010), In-service diagnostics of a highway bridge from a progressive damage case study, *ASCE Journal of Bridge Engineering*, **15**(5), 597–607.

Xu, B., Chen, G. & Wu, Z. (2007), Parametric identification for a truss structure using axial strain, *Computer-Aided Civil and Infrastructure Engineering*, **3**(22), 210–22.